Journal of Magnetism and Magnetic Materials 560 (2022) 169620

Contents lists available at ScienceDirect

Journal of Magnetism and Magnetic Materials

journal homepage: www.elsevier.com/locate/jmmm

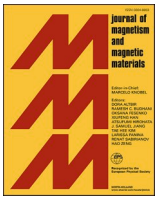

Equiatomic quaternary CoXCrAl (X = V, Nb, and Ta) Heusler compounds: Insights from DFT calculations

Tugce Sevinc Dag [a], Aysenur Gencer [b,*], Yasemin Ciftci [c], Gokhan Surucu [d,e]

[a] Department of Physics, Graduate School of Natural and Applied Sciences, Gazi University, Ankara 06500, Turkey
[b] Department of Physics, Karamanoglu Mehmetbey University, Karaman 70100, Turkey
[c] Department of Physics, Gazi University, Ankara 06500, Turkey
[d] Department of Energy Systems Engineering, Gazi University, Ankara 06500, Turkey
[e] Department of Electric and Energy, Ahi Evran University, Kırşehir 40100, Turkey

ARTICLE INFO

Keywords:
Half metals
Equiatomic quaternary Heusler compounds
Density functional theory

ABSTRACT

The half-metallic ferromagnets are likely materials to the spintronics systems for the next generation electronic devices. Among the half-metallic ferromagnetic materials, the equiatomic quaternary Heusler (EQH) compounds get great attention in the recent times. In this study, the EQH CoXCrAl (X = V, Nb, and Ta) compounds are investigated using Density Functional Theory (DFT). The three structural types as type-I, type-II, and type-III, are considered to determine the most stable structural types of CoXCrAl compounds. Furthermore, the three magnetic configurations as paramagnetic (PM), ferromagnetic (FM), and antiferromagnetic (AFM), are studied to find out the most stable magnetic configuration. The type-I FM configuration is the most stable configuration for the CoXCrAl compounds. The calculated electronic band structures reveal that the CoXCrAl compounds are half-metals with metallic behavior in spin-up channel and semiconducting behavior in spin-down channel. Also, the possible d-d hybridizations between the Co, X, and Cr atoms are investigated to show the half-metallic character in detail. Furthermore, the calculated elastic constants satisfy the Born stability criteria, then the CoXCrAl compounds have mechanical stability. Using the determined constants, the mechanical properties are obtained for CoXCrAl compounds. In addition, the dynamical properties are studied and it is found that CoXCrAl compounds are dynamically stable. The structural, magnetic, electronic, mechanic and dynamical properties of CoXCrAl compounds that are the potential candidates for the spintronics applications are presented in this study.

1. Introduction

In recent years, the electronic devices are an indispensable part of daily routine. With the increasing usage of these devices, there have been occurring requirements such as storage of more data, reducing the device size, less power consumption, etc. The spintronics, also known as spin electronics, is an encouraging field for the next generation electronic devices that meets these requirements [1]. In the spintronics, the spin of electrons is used for the electronic device similar to the charge of the electron in the standard electronic devices [2]. The half-metallic ferromagnets are the most compatible materials for the spintronics applications [3]. In 1983, Groot et al. [4] discovered the half metallicity in Mn based Heusler compounds. In half metal compounds, the metallic behavior is observed in one spin channel and the semiconducting behavior is observed in the other spin channel [5]. Therefore, these compounds have 100% spin polarization at the Fermi level that is fundamental for the spintronics applications.

The Heusler compounds have been considered as suitable materials for the spintronics applications due to their half metallic behavior among other half metallic materials such as double perovskites [6,7], CrO_2 [8], etc. The Heusler compounds are defined in three types as; full-Heusler [9,10], half-Heusler [11,12] and quaternary Heusler [13,14]. The full-Heusler, hall-Heusler and quaternary Heusler can be described with their stoichiometric ratios as follows, X_2YZ, XYZ, and XX'YZ, respectively. In here, X, X', and Y are transition metals and Z is the main group element [15]. The equiatomic quaternary Heusler compounds (EQHCs) [16] have the cubic structure with the space group $F\bar{4}3m$, *#216* [17]. The EQHCs get great attention due to their remarkable properties such as ferromagnetism, half metallic characteristics, good thermoelectric performance, etc. Although, some experimental studies

* Corresponding author.
E-mail address: aysenurgencer@gmail.com (A. Gencer).

https://doi.org/10.1016/j.jmmm.2022.169620
Received 8 April 2022; Received in revised form 9 June 2022; Accepted 14 June 2022
Available online 17 June 2022

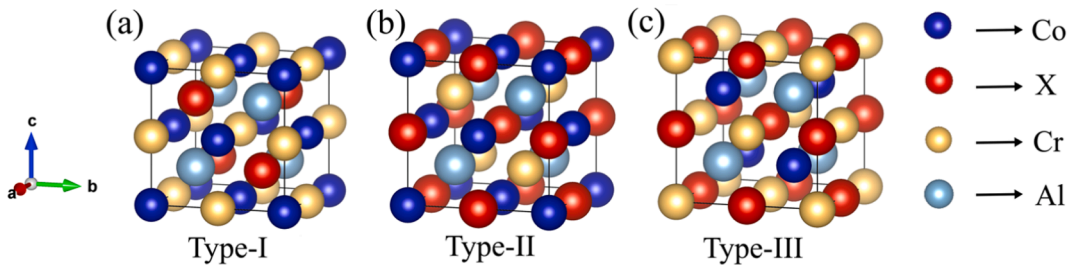

Fig. 1. Three-dimensional lattice of (a) Type-I, (b) Type-II, and (c) Type-III phases of CoXCrAl (X = V, Nb, Ta) compounds.

[18–20] have been performed for the EQHCs, the more attention is received for the theoretical studies being less expensive and well efficient to lead the experimental studies [21,22].

In the literature, CrLaCoZ (Z = Al, Ga, In, Ge, Sn, Pb) quaternary Heusler alloys have been studied by Liu et. al. [22] and it has been found that these compounds are half metals obeying the Slater-Pauling rule for their magnetic moments. CoZrCrZ (Z = Al, Ga, In) Heusler compounds have been considered by Priyanka et. al. [5] and they have obtained the electronic, mechanic, and thermoelectric properties of these compounds. Also, CoScCrZ (Z = Al, Ga, Ge, In) Heusler alloys have been investigated for the various physical properties by Shakil et. al [23] and the determined properties show that these compounds are possible candidates for spintronics and thermoelectric applications. In addition to these studies, CoNbCrZ (Z = Al, Ga, Si, Ge) [14] and NbCoCrAl and NbRhCrAl [24] have been studied recently. These studies have considered X, X', and Y atoms as Co, Nb, and Cr and the X' atom could be chosen as V and Ta where they are located above Nb and below Nb on the periodic table, respectively. Therefore, CoXCrAl (X = V, Nb, and Ta) EQHCs have been considered in this study. Density Functional Theory (DFT) calculations have been performed for the structural, electronic, mechanic, and dynamical properties of these compounds and the results for CoVCrAl and CoTaCrAl have been presented for the first time as far as known studies in the literature. In addition, this study presents the mechanical and dynamical properties of CoXCrAl EQHCs in detail as well as their electronic properties which are usually considered in the studies found in the literature. The complete investigation of the mechanical, dynamical, and electronic properties of these compounds will be a leading study for future experimental works.

2. Calculation details

In this study, the Vienna Ab-initio Simulation Package (VASP) [25,26] is used for density functional theory (DFT) calculations which is the most common method used to determine ground state properties of materials. The Perdew, Burke and Ernzerhof (PBE) functional [27] in the Generalized Gradient Approximation (GGA) is employed to describe the exchange–correlation energy for electron–electron interactions. For the electron–ion interactions, the Projector Augmented Wave (PAW) method [28,29] is used. The DFT calculations are employed with a Γ-centered Monkhorst-Pack scheme [30] **k**-points mesh of 18 × 18 × 18 and a 500 eV cut-off energy for the optimization of CoXCrAl (X = V, Nb, and Ta) compounds. Moreover, the energy and force convergence tolerances are set as 1×10^{-11} eV per atom and 1×10^{-6} eV/Å, respectively. Moreover, the valence electron configurations of Co, V, Nb, Ta, Cr and Al atoms are employed as $3d^8 4s^1$, $3d^4 4s^1$, $4d^4 5s^1$, $5d^3 6s^2$, and $3s^2 3p^1$, respectively. The stress–strain method implemented in the VASP [31] is used to calculate the mechanical properties of these compounds and the ionic contribution is also considered for the elastic constants calculations. The ELATE software [32] is used for the three dimensional schematic representations of mechanical properties. The sound wave velocities are calculated using the Christoffel software [33]. The phonon distribution curves and thermal properties of compounds are examined using linear response method employing a 2 × 2 × 2 supercell created with PHONOPY software [34].

3. Results and discussions

3.1. Structural and magnetic properties

In this study, three different structural phases, type-I, type-II, and type-III, are examined that are the only possible configurations of CoXCrAl (X = V, Nb, and Ta) EQHCs. The schematic representations of the compounds are shown in Fig. 1. The Co, X, Cr, and Al atoms are located at 4a, 4b, 4c, and 4d Wyckoff positions for type-I while they are located at 4a, 4c, 4b, and 4d Wyckoff positions for type-II, respectively. For type-III structure, the Co, X, Cr, and Al atoms are located at 4b, 4c, 4a and 4d, respectively. The CoXCrAl compounds are optimized and the obtained lattice parameters, partial and total magnetic moments and the calculated formation energies are listed in Table 1. The calculated lattice parameter for CoNbCrAl is coherent with the available literature as listed in Table 1. However, the lattice parameters for CoVCrAl and CoTaCrAl cannot be compared due to no results for CoVCrAl and

Table 1
Lattice constants (a in Å), formation energies (ΔE_f in eV/atom), total magnetic moments (M_t in μ_B), and partial magnetic moments of atoms (M_{Co}, M_X, and M_{Cr} in μ_B) for CoXCrAl (X = V, Nb, and Ta) compounds in the type-I, type-II, and type-III phases.

Compound	Phase	a	ΔE_f	M_t	M_{Co}	M_X	M_{Cr}
CoVCrAl	Type-I	5.816	−0.258	−0.966	−0.315	0.485	−1.141
	Type-II	5.848	−0.104	−0.785	−0.411	−1.339	0.977
	Type-III	5.939	−0.037	−4.340	−1.255	−0.471	−2.614
CoNbCrAl	Type-I	6.023	−0.186	−0.951	−0.121	0.170	−1.006
		6.018 [14]		0.993 [14]	0.158 [14]	−0.119 [14]	0.887 [14]
		6.020 [24]			0.060 [24]	−0.160 [24]	1.080 [24]
	Type-II	6.053	0.049	−1.771	−1.015	−0.065	−0.709
		6.049 [14]					
	Type-III	6.153	−0.035	−4.397	−1.398	0.049	−3.044
		6.149 [14]					
CoTaCrAl	Type-I	5.997	−0.245	−0.959	−0.143	0.082	−0.903
	Type-II	6.052	0.085	−1.841	−1.069	−0.048	−0.742
	Type-III	6.133	−0.017	−4.326	−1.390	0.066	−2.993

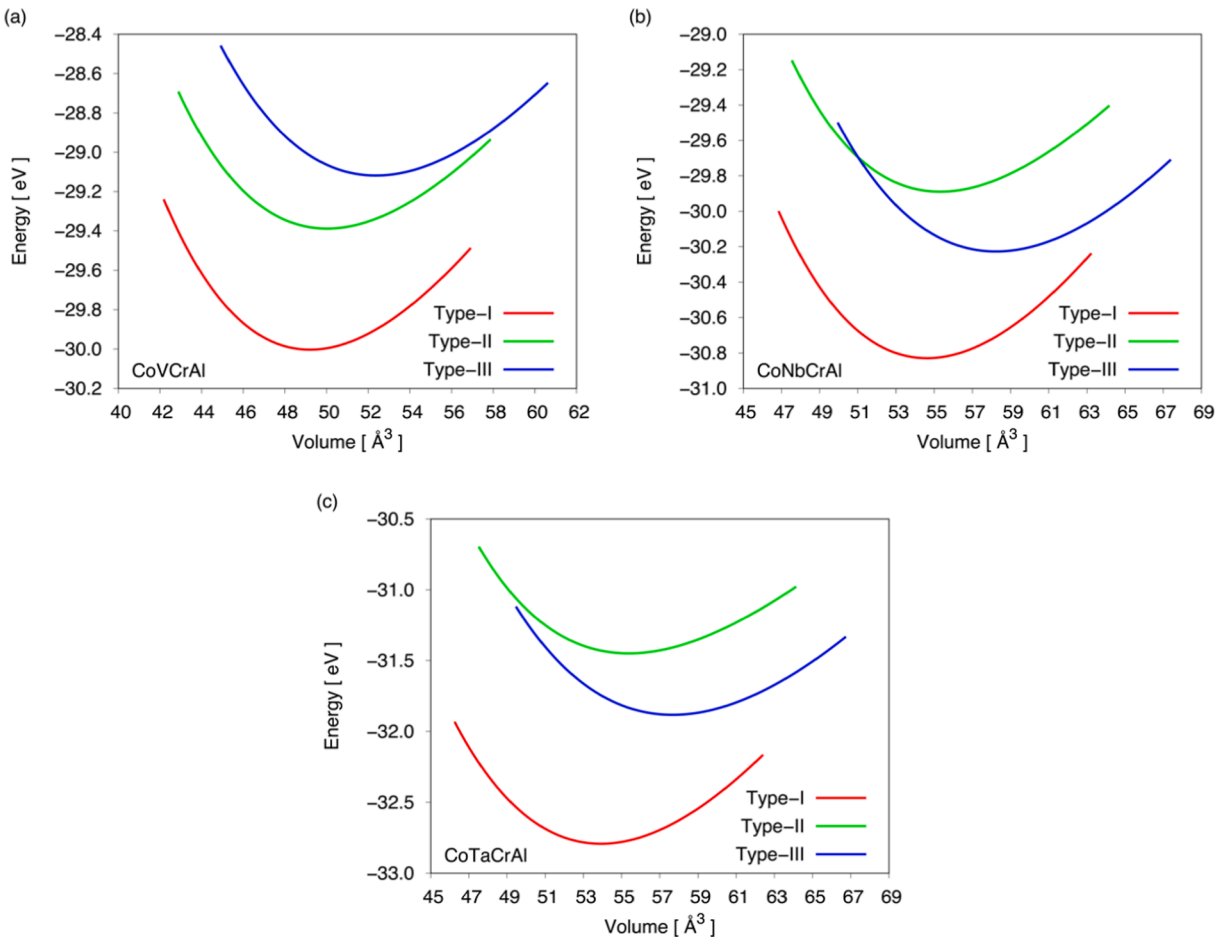

Fig. 2. Energy change with respect to volume for (a) CoVCrAl (b) CoNbCrAl and (c) CoTaCrAl compounds for type-I, type-II, and type-III phases.

CoTaCrAl in the literature. If one compares the lattice parameters for different types, it can be found that the type-III phase has the greatest one for these compounds. In addition, the order of lattice parameter is CoNbCrAl > CoTaCrAl > CoVCrAl that is resulted from the bond lengths between these atoms as listed in Table S1.

The formation energies [35] are calculated with Equation (1) where $E^{CoXCrAl}$ is the total energy of CoXCrAl compound and E^{Co}, E^{X}, E^{Cr} and E^{Al} are the ground state energies of one Co, X, Cr, and Al atoms obtained from the bulk form, respectively. A negative formation energy indicates that the material is structurally stable and experimentally synthesizable. In addition, if it is desired to make a comparison between these calculated values, it can be said that the lower value is more favorable energetically than the high one. It is seen that the type-I phase is the most stable for all CoXCrAl compounds according to the calculated formation energies. In addition, the convex hull distance is another indicator for the experimental synthesizability of materials and it is defined as the difference between hull energy and formation energy. The convex hull distance less than 0.1 eV/atom implies the experimental synthesizability for the quaternary Heusler compounds [36] and also, it is reported that a convex hull distance ~ 0.2 eV/atom is occurred for some synthesized compounds and it is indicating metastability [37,38]. The convex hull distances for CoXCrAl compounds are obtained from the Open Quantum Materials Database (OQMD) [39,40]. The convex hull distances are 0.143 eV/atom, 0.189 eV/atom and 0.184 eV/atom for CoVCrAl, CoNbCrAl and CoTaCrAl, respectively. Therefore, these compounds are also synthesizable as a metastable phase according to the convex hull distances.

$$\Delta E_f = E^{CoXCrAl} - (E^{Co} + E^{X} + E^{Cr} + E^{Al}) \quad (1)$$

In Table 1, the calculated magnetic moments are listed and the Slater-Pauling rule [41] could be used to determine these magnetic moments theoretically using the number of valence electrons. According to the Slater-Pauling rule, the total magnetic moment for a quaternary Heusler compound could be determined using Equation (2) where M_{tot} is the total magnetic moment per formula unit and N_V is the number of total valence electrons.

$$M_{tot} = (N_V - 24)\mu_B \quad (2)$$

The number of valence electrons is 23 for CoXCrAl compounds, and the calculated magnetic moments for type-I phase, the most stable phase, are $-0.966\ \mu_B$, $-0.951\ \mu_B$, and $-0.959\ \mu_B$ for CoVCrAl, CoNbCrAl, and CoTaCrAl, respectively. These magnetic moments are consistent with the expected $-1\mu_B$ value according to the Slater-Pauling rule. In literature, Reference [14] and [24] take the Slater-Pauling rule as $(24 - N_V)\mu_B$ and they found the total magnetic moment as $0.993\ \mu_B$ but if they used Equation (2), they would get the total magnetic moment value around $-1\ \mu_B$ that is consistent with the presented results as $-0.951\ \mu_B$ in Table 1.

The type-I phase is the most stable phase for these compounds according to the formation energy calculations. In addition to these calculations, the total energy change with respect to volume is obtained as shown in Fig. 2. The type-I phase, the lowest lying curve, is the most stable phase as can be seen from Fig. 2 that is consistent with the results from the formation energy.

In addition to consideration of different structural phases, the CoXCrAl compounds are considered for the magnetic configurations as paramagnetic (PM), ferromagnetic (FM) and antiferromagnetic (AFM) to decide the stable magnetic configuration in addition to the

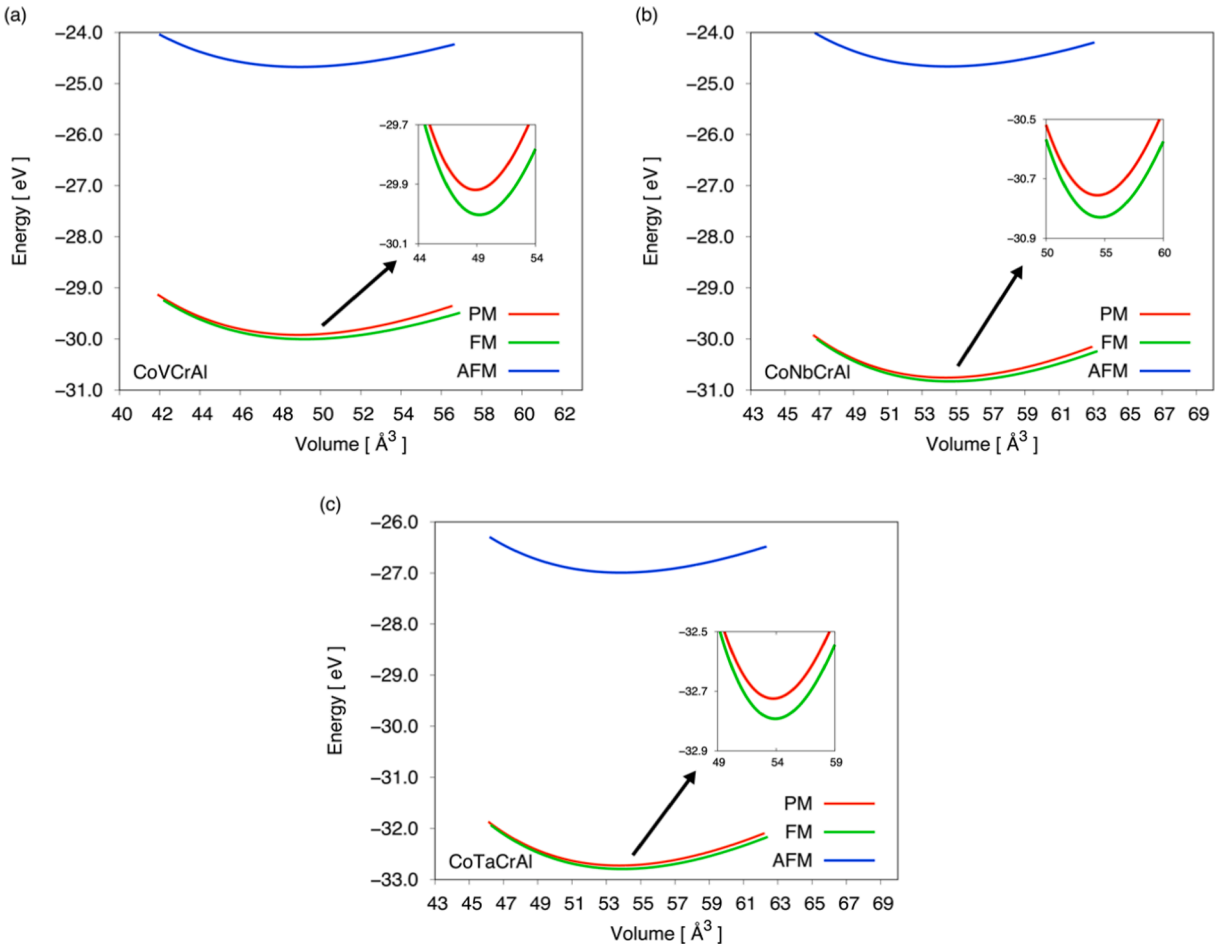

Fig. 3. Energy change with respect to volume for (a) CoVCrAl, (b) CoNbCrAl, and (c) CoTaCrAl compounds for type-I PM, FM, and AFM phases.

structurally stable phase. Fig. 3 presents the energy evolution with the volume change for PM, FM and AFM configurations and it can be seen that the most stable configuration is FM. Also, the insets in Fig. 3 shows the difference between PM and FM configurations in detail. Therefore, the type-I FM phase is considered in the subsequent sections.

3.2. Electronic properties

The electronic properties of CoXCrAl (X = V, Nb, and Ta) EQHCs are investigated with the calculation of the band structure and partial density of states (DOS) as shown in Fig. 4. The spin-polarized electronic band structure of CoXCrAl compounds show that these compounds exhibit a metallic character in the spin-up channel, while semiconducting character with a band gap in the spin-down channel. Therefore, equiatomic quaternary Heusler CoXCrAl compounds are half metals with 0.161 eV, 0.167 eV and 0.142 eV band gaps in spin-down channel for CoVCrAl, CoNbCrAl and CoTaCrAl, respectively. Also, the middle part in the band structure shows the density of states and as can be seen from Fig. 4, the most contributions come from Cr and Al atoms above the Fermi level and below the Fermi level, respectively. Furthermore, the detailed partial density of states are given in Fig. 4 and it is concluded that the d orbitals of Co, V, Nb, Ta, Cr and p orbitals of Al atoms give more contributions to the partial DOS. The CoXCrAl EQHCs with FM half metallic character have a considerable potential to applied in the spintronics applications.

Özdoğan et. al. [41] considered the principle of the half-metallic character of the EQHCs that have only one magnetic atom. The CoXCrAl compounds having more than one magnetic atom, could be considered with this interpretation to discuss the half-metallic character of the CoXCrAl compounds. Fig. 5 shows the probable hybridizations of the d-d orbitals of Co, X and Cr atoms. Besides, the contribution to the band gap formation from the s and p orbitals is minor due to location at lower energies than d orbitals [42,43]. The Co, X, and Cr atoms have five d orbitals being double (d_{z^2} and $d_{x^2-y^2}$) and triple (d_{xy}, d_{yz}, and d_{zx}) degenerated. In the CoXCrAl compounds, there are five bonding and five anti-bonding orbitals resulted from the hybridizations of the d orbitals of the Co and X atoms. In these orbitals, the double degenerated bonding e_g and anti-bonding e_u orbitals are created with the hybridizations of the double degenerated d orbitals of Co and X atoms while triple degenerated bonding t_{2g} and anti-bonding t_{1u} orbitals are created with the hybridizations of the triple degenerated d orbitals of Co and X atoms. After these hybridizations, these bonding and anti-bonding orbitals hybridize with the d orbitals of Cr atoms with the generation of e_g and t_{2g} bonding orbitals located at lower energy and e_g and t_{2g} anti-bonding orbitals located at higher energy as shown in Fig. 5. The hybridizations of Co - X and Cr atoms yield with bonding and anti-bonding orbitals with $E(e_g) < E(t_{2g})$ due to the location of the Co and X atoms being at the center of Cr tetrahedron. In addition, the anti-bonding orbitals of Co - X hybridizations do not hybridize with the Cr atoms and these orbitals are located at the same energy level. Therefore, CoXCrAl compounds are half-metals. To visualize these hybridizations that are shown schematically in Fig. 5, the detailed density of states are shown in Fig. 6a and Fig. 6b for e_g and t_{2g} orbitals of Co and V atoms and of Co-V and Cr atoms, respectively. In Fig. 6a, the t_{2g} orbitals of Co and V atoms hybridize between −1.50 and −1.30 eV and the e_g orbitals of these atoms hybridize between 1.00 and 1.20 eV in the spin-down orientation. For the hybridizations between Co-V and Cr atoms, the t_{2g} orbitals hybridize between −1.20 and 0.00 eV and the e_g orbitals hybridize between 0.60

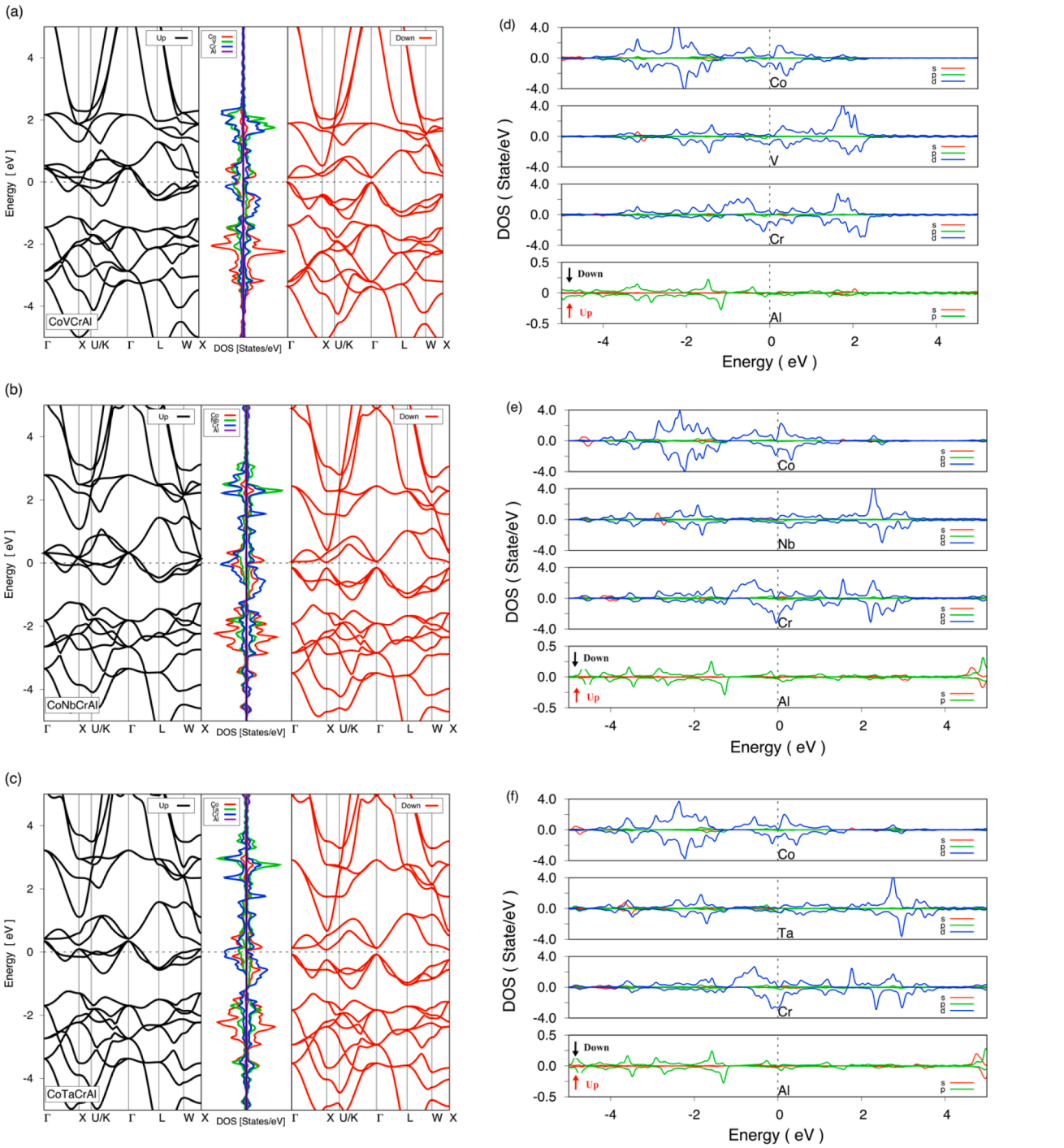

Fig. 4. The electronic band structures for (a) CoVCrAl, (b) CoNbCrAl, (c) CoTaCrAl and partial density of states for (d) CoVCrAl, (e) CoNbCrAl and (f) CoTaCrAl.

and 1.10 eV in the spin-down orientation as shown in Fig. 6b.

3.3. Mechanic and dynamical properties

Elastic constants of a material provide information about the mechanical properties and mechanical stability of a material. The elastic constants for equiatomic quaternary Heusler CoXCrAl (X = V, Nb, and Ta) compounds are calculated and listed in Table 2. Three elastic constants as C_{11}, C_{12} and C_{44} are listed in Table 2 that are the necessary constants for the cubic crystal systems. These elastic constants should satisfy the Born stability criteria [44,45] as given in Equation (3) and if these criteria are satisfied, it could be concluded that the compound has the mechanical stability.

$$C_{11}-C_{12}>0$$
$$C_{11}+2C_{12}>0 \quad (3)$$
$$C_{11}>0,\ C_{44}>0$$

The listed elastic constants in Table 2 satisfy the Born stability criteria that indicates the mechanical stability of CoXCrAl compounds. In addition to the elastic constants, the Cauchy pressure are listed in Table 2. A negative value for the Cauchy pressure indicates the brittleness while a positive value indicates the ductility. As concluded from Table 2, the CoXCrAl compounds are ductile materials having positive

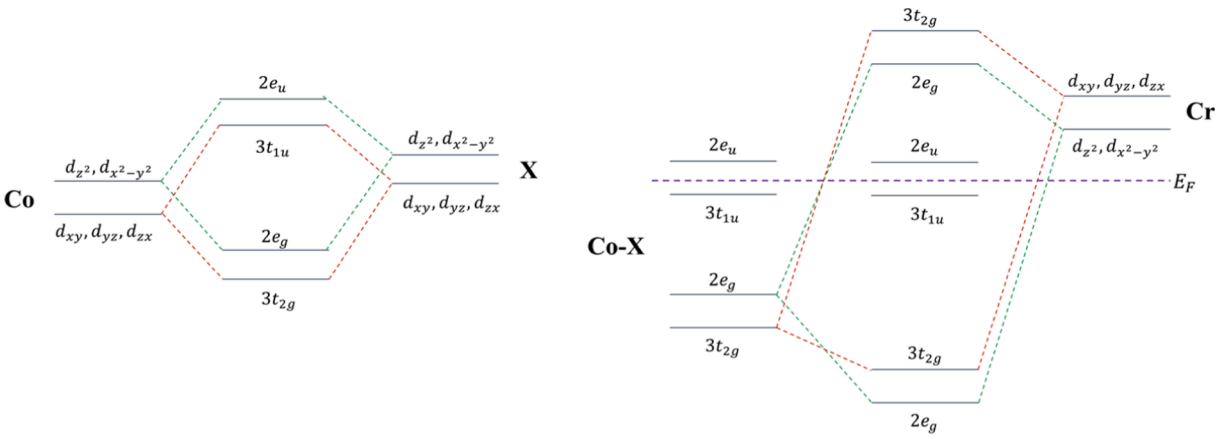

Fig. 5. The schematic representations of possible d-d hybridization for CoXCrAl compounds.

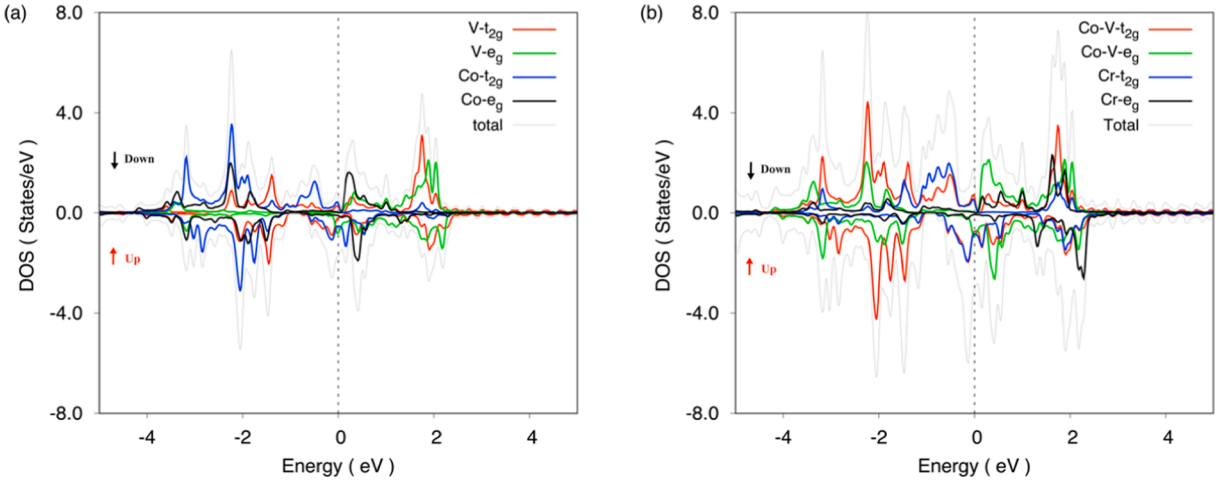

Fig. 6. The partial density of states using e_g and t_{2g} states for (a) Co and V atoms and (b) Co-V and Cr atoms.

Table 2
Elastic constants (C_{ij} in GPa), and Cauchy pressure ($C_p = C_{12}$-C_{44} in GPa) for CoXCrAl (X = V, Nb, and Ta) compounds.

Compound	C_{11}	C_{12}	C_{44}	C_p
CoVCrAl	291.312	132.936	110.518	22.418
CoNbCrAl	265.323	143.834	92.628	51.207
	173.300 [14]	117.200 [14]	62.800 [14]	
CoTaCrAl	270.765	157.318	99.971	57.347

Cauchy pressures. In Table 2, the results for CoNbCrAl [14] are also listed and these results are lower than the results obtained in this study. In this study, the elastic constants of CoNbCrAl are determined with the ionic contribution that provides detailed consideration for this compound. So, the difference between Ref. [14] and this study could be due to the disparate calculation methods. Furthermore, CoNbCrAl has the lowest elastic constants among these compounds consistent with the highest lattice parameter and it has the lowest hardness among these compounds. This is due to the longer bond lengths in CoNbCrAl than in CoVCrAl and CoTaCrAl compounds.

The calculated elastic constants could be employed to obtain the mechanical properties like bulk modulus, shear modulus, etc. to demonstrate the technological applications for the CoXCrAl compounds. Table 3 lists the bulk (B) and shear (G) moduli for the CoXCrAl compounds determined with the Voight [46] – Reuss [47] – Hill [48] approximations using the calculated elastic constants in Table 2. In these approximations, the upper, lower and average values are calculated using Voight, Reuss, and Hill approximations, respectively. The listed bulk and shear moduli in Table 3 are the results from the Hill approximation which gives the closer values to the experimental results. Using these bulk and shear moduli, Young's modulus, Poisson's ratio, G/B and B/G ratios are obtained and listed in Table 3 as well. According to Table 3, CoTaCrAl has the highest bulk modulus among these compounds. Therefore, it has the highest resistance to the volume change

Table 3
The bulk modulus (B in GPa), shear modulus (G in GPa), Young's modulus (E in GPa), Poisson's ratio (υ), G/B ratio, and B/G ratio for CoXCrAl (X = V, Nb, and Ta) compounds.

Compound	B	G	E	υ	G/B	B/G
CoVCrAl	185.728	96.702	247.203	0.278	0.521	1.921
CoNbCrAl	184.330	78.215	205.568	0.314	0.424	2.357
	135.900 [14]	45.450 [14]	122.670 [14]	0.340 [14]		2.900 [14]
CoTaCrAl	195.134	79.640	210.308	0.320	0.408	2.450

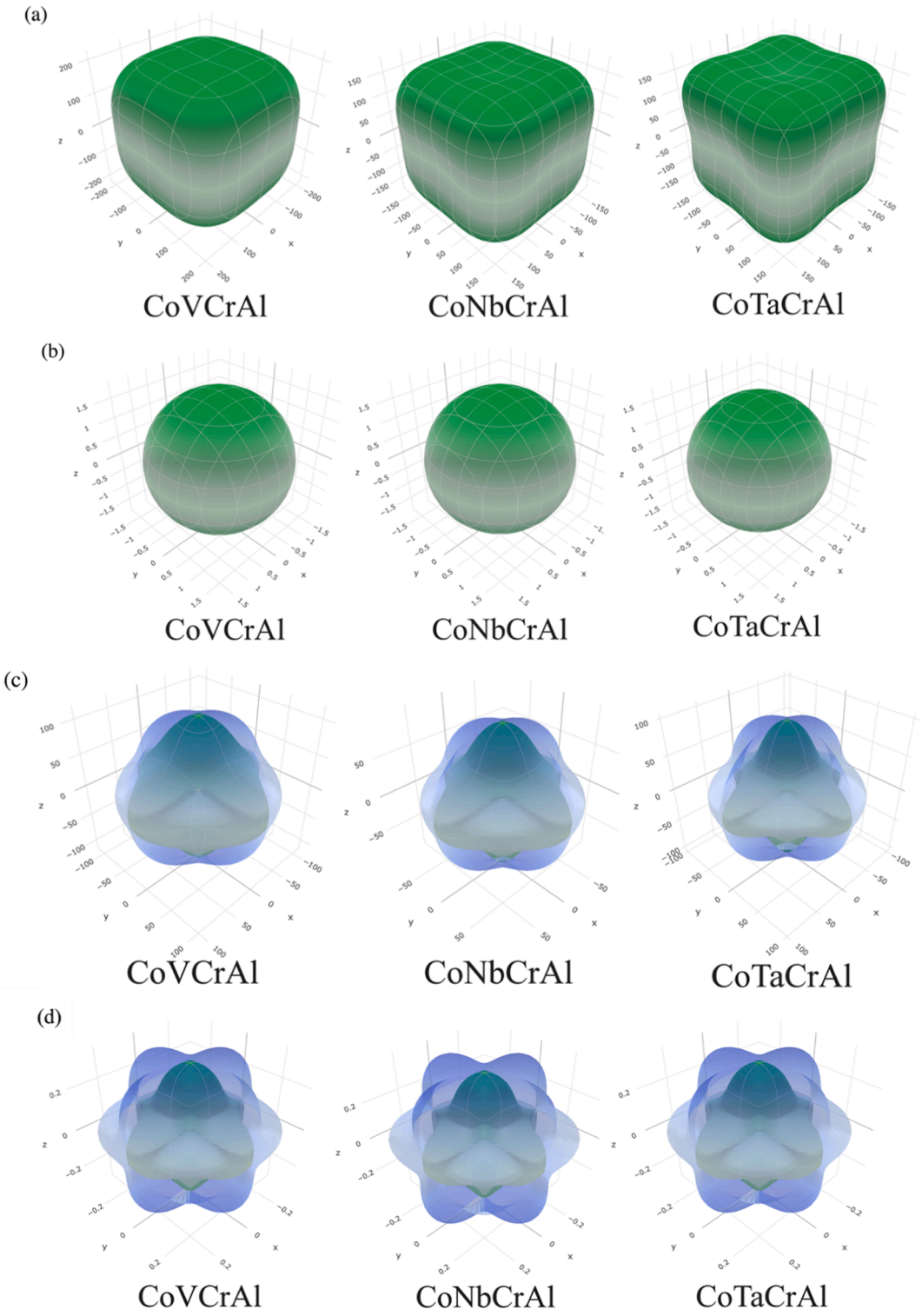

Fig. 7. The three-dimensional directional dependence of (a) Young's modulus, (b) linear compressibility, (c) shear modulus, and (d) Poisson's ratio for CoCrAl (X = V, Nb, and Ta) compounds.

when a hydrostatic pressure is employed. Besides, CoVCrAl has the highest shear and Young's moduli that indicates the highest resistance to plastic deformations and highest stiffness among these compounds. The Poisson's ratio is an essential parameter to determine the bonding nature of a material and it is the length change in the perpendicular direction when a push or pull applied. The dominantly ionic bonding materials have the Poisson's ratio around 0.25 while the dominantly covalent bonding materials have the Poisson's ratio around 0.1 [49]. The CoXCrAl compounds have dominantly ionic bonding as concluded from the listed Poisson's ratios in Table 3. Another essential parameter for the determination of the bonding type of a material is G/B ratio and if the G/B ratio is around 0.6, it indicates the dominantly ionic bonding while if it is 1.1, it indicates the covalent bonding [49]. The CoXCrAl compounds have dominantly ionic bonding having the G/B ratios around 0.6 that is consistent with the results of the Poisson's ratios. Like the Cauchy pressure, the B/G ratio could be used to determine the

Table 4
The longitudinal (V_L in m/s), transverse (V_T in m/s), and average (V_M in m/s) wave velocities, the minimum thermal conductivities (λ_{min} in W/m K) using Cahill, Clarke and Long models and the diffusion thermal conductivities (λ_{diff} in W/m K) for CoXCrAl (=V, Nb, and Ta) compounds.

Compound	V_L	V_T	V_M	λ_{min}			λ_{diff}
				Cahill Model	Clarke Model	Long Model	
CoVCrAl	7025	3894	4338	1.403	1.547	1.128	0.872
CoNbCrAl	6413	3339	3736	1.250	1.378	1.005	0.776
	2490 [14]	5195 [14]	3090 [14]				
CoTaCrAl	5539	2848	3189	1.063	1.173	0.855	0.660

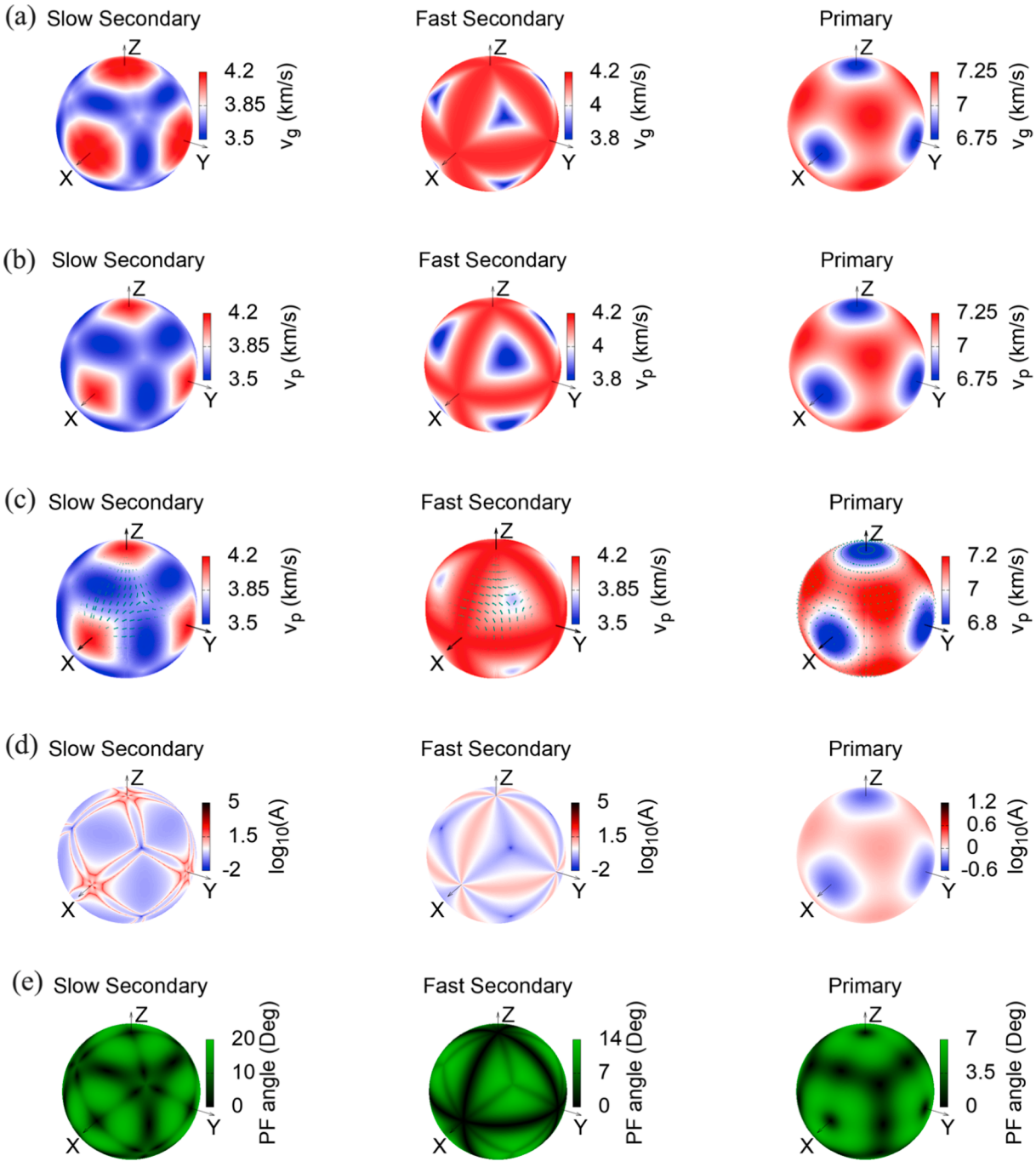

Fig. 8. (a) Group velocity, (b) phase velocity, (c) polarization of sound waves, (d) enhancement factor and (e) power flow angle for the CoVCrAl compound.

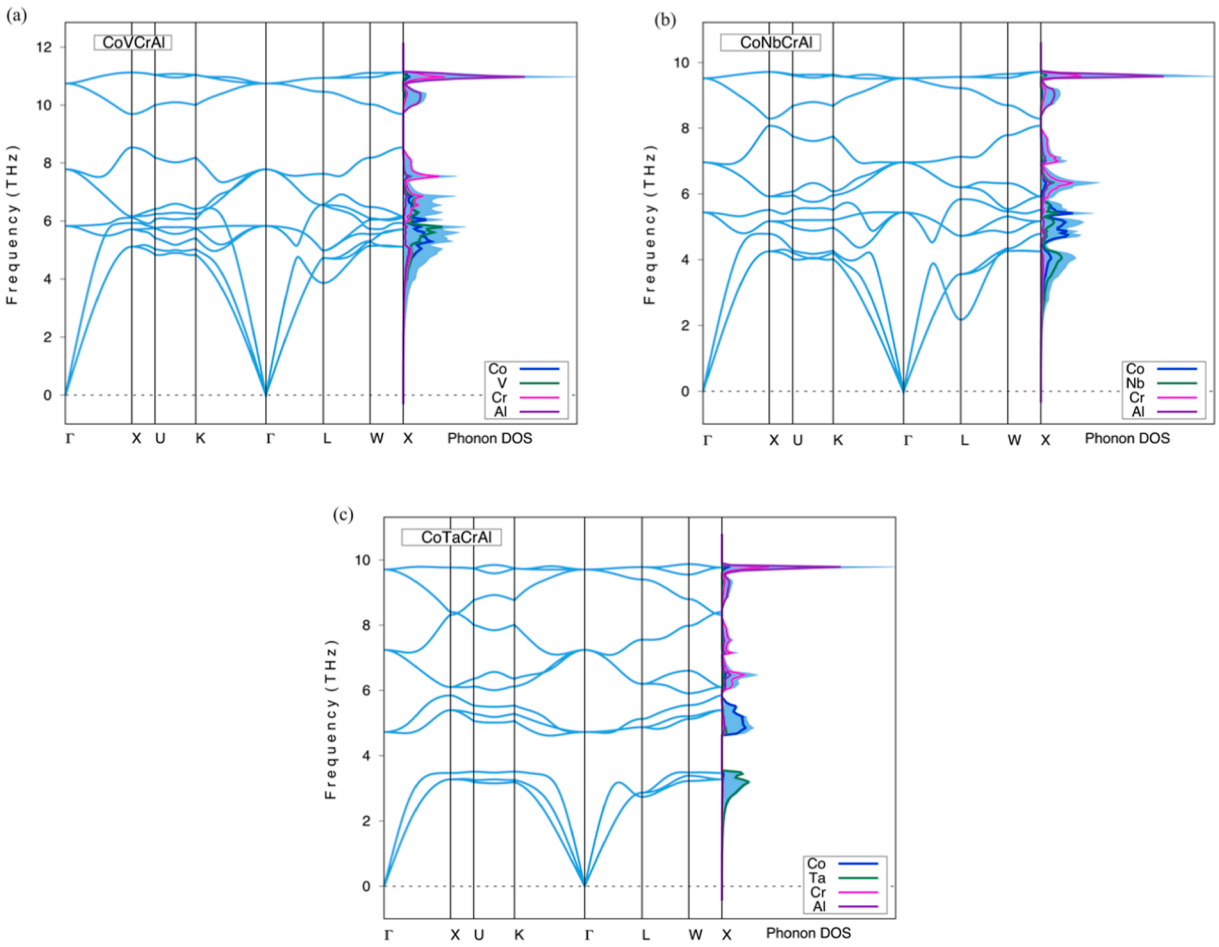

Fig. 9. Phonon dispersion curves with the phonon density of states (DOS) (a) CoVCrAl, (b) CoNbCrAl and (c) CoTaCrAl compounds.

ductility or brittleness. For this determination, 1.75 value is crucial and if the B/G ratio is higher than this value, it indicates the ductility while if it is lower, it indicates the brittleness [49]. The CoXCrAl compounds are ductile materials having the B/G ratios larger than 1.75 and this result is coherent with the result from the Cauchy pressure.

In addition to the listed mechanical properties in Table 3, the three-dimensional directional dependence for Young's modulus, linear compressibility, shear modulus and Poisson's ratio for CoXCrAl compounds are shown in Fig. 7 obtained using ELATE software [32]. These directional dependences are crucial to determine the anisotropic characteristics that give information for microcracks, plastic deformations, etc. The spherical shapes indicate the isotropy while the distorted shapes indicate the anisotropy in the three-dimensional directional dependence displays. As can be seen from Fig. 7, the linear compressibility is isotropic and the remaining parameters are anisotropic. In addition, the green shapes show the minimum values while the blue ones show the maximum values of these parameters in Fig. 7 and the values are listed in Table S2.

The equations given in [50] could be applied to obtain the longitudinal, transverse and average wave velocities using the determined bulk and shear moduli. The obtained longitudinal, transverse and average wave velocities for CoXCrAl compounds are listed in Table 4 and CoVCrAl has the highest longitudinal, transverse and average wave velocities among these compounds. Furthermore, the minimum and diffusion thermal conductivities for CoXCrAl compounds are listed in Table 4. The minimum thermal conductivities are determined using Cahill model [51], Clarke model [52] and Long model [53] while the Synder model [54] is employed to determine the diffusion thermal conductivities. As listed in Table 4, the Clarke model gives the higher thermal conductivities for these compounds among these models. In addition, CoVCrAl has the highest minimum and diffusion thermal conductivities among these compounds that is consistent with the highest wave velocities of this compound.

The sound wave velocities of CoXCrAl compounds are obtained using the Christoffel software [33] and Fig. 8 shows the group velocity, phase velocity, phase polarization, enhancement factor and power flow angle for CoVCrAl. Figures for CoNbCrAl and CoTaCrAl are available in Fig. S1 and Fig. S2, respectively. In Fig. 8, the slow secondary and fast secondary spheres show the transverse wave velocities, while the primary sphere shows the longitudinal wave velocity. The group wave velocity along the x, y, and z axes have higher velocities for the slow secondary and fast secondary phases and lower velocities for the primary phase. Similar behavior is observed for phase wave velocities in Fig. 8b. In Fig. 8c, the transverse polarization is occurred in the primary mode and the longitudinal polarization is occurred in the secondary modes. The enhancement factor is the ratio of the direction of the group wave velocity to the direction of the phase wave velocity and has higher values for the secondary phases along the x, y, and z axes and lower values for the primary phase along the same directions. The power flow angle is the angle between the group wave velocity and the phase wave velocity and all phases have low values along the x, y, and z axes. In addition, similar results are observed for CoNbCrAl and CoTaCrAl compounds.

The phonon dispersion curves of CoXCrAl compounds are presented in Fig. 9 with the phonon density of states (DOS). The CoXCrAl compounds have 4 atoms in their unit cell, so there are 12 phonon branches in Fig. 9 where 3 of them are acoustic phonon branches and the remaining branches are optic phonon branches. In addition, there is no negative frequency called soft mode that indicates the dynamically

stability for these compounds. The phonon DOS presents that the Al atoms contribute more to higher frequencies due to the smaller atomic mass than other atoms in these compounds. Furthermore, the thermal properties as entropy, free energy and heat capacity change with respect to temperature are presented in Fig. S3. As can be seen from Fig. S3, the entropy increases with the temperature increment while the free energy decreases. Also, the heat capacity has a sharp increase at low temperature and it reaches a constant called Dulong-Petit limit at the high temperatures.

4. Conclusion

In this study, the structural, mechanical, magnetic, electronic and dynamic properties of equiatomic quaternary Heusler CoXCrAl (X = V, Nb, and Ta) compounds are investigated using Density Functional Theory. The three different structural phases are studied for these compounds and it has been found that type-I is the most stable phase. Among the three different magnetic configurations as ferromagnetic (FM), paramagnetic (PM) and antiferromagnetic (AFM) are investigated for type-I phase and it is revealed that the FM phase is the most stable. The magnetic moments of the compounds are determined as −0.966, −0.951 and −0.959 for CoXCrAl (X = V, Nb, Ta) compounds, and they are consistent with the Slater-Pauling rule. The electronic band structures show that these compounds are half metals. In addition, the hybridizations between the d orbitals of Co, X and Cr atoms are examined to reveal the half metallic character of these compounds. These compounds are mechanically stable according to the calculated elastic constants. Furthermore, the studied mechanical properties show that these compounds exhibit a ductile behavior and have dominantly ionic bonding. The three-dimensional directional dependence of Young's modulus, linear compressibility, shear modulus and Poisson's ratio show that the linear compressibility is isotropic, while the Young's modulus, shear modulus and Poisson's ratio are anisotropic. In addition to these mechanical properties, the minimum thermal conductivities are obtained and the sound wave velocities are calculated and visualized in 3D. Furthermore, the phonon dispersion curves having no soft modes show that these compounds are also dynamically stable. Therefore, these detailed structural properties especially their FM half-metallic character, indicate that the CoXCrAl (X = V, Nb, Ta) compounds are potential candidates for the spintronics applications.

CRediT authorship contribution statement

Tugce Sevinc Dag: Data curation, Investigation, Writing – original draft. **Aysenur Gencer:** Conceptualization, Investigation, Writing – original draft. **Yasemin Ciftci:** Investigation, Formal analysis, Writing – review & editing. **Gokhan Surucu:** Conceptualization, Methodology, Validation, Writing – review & editing.

Declaration of Competing Interest

The authors declare that they have no known competing financial interests or personal relationships that could have appeared to influence the work reported in this paper.

Acknowledgements

The DFT calculations were fully performed at TUBITAK ULAKBIM, High Performance and Grid Computing Center (TRUBA resources).

Appendix A. Supplementary material

Supplementary data to this article can be found online at https://doi.org/10.1016/j.jmmm.2022.169620.

References

[1] A. Hirohata, K. Yamada, Y. Nakatani, I.-L. Prejbeanu, B. Diény, P. Pirro, B. Hillebrands, Review on spintronics: Principles and device applications, J. Magn. Magn. Mater. 509 (2020) 166711.
[2] C. Felser, G.H. Fecher, B. Balke, Spintronics: A Challenge for Materials Science and Solid-State Chemistry, Angew. Chem. Int. Ed. 46 (2007) 668–699, https://doi.org/10.1002/ANIE.200601815.
[3] A.Q. Seh, D.C. Gupta, Quaternary Heusler alloys a future perspective for revolutionizing conventional semiconductor technology, J. Alloy. Compd. 871 (2021), 159560, https://doi.org/10.1016/J.JALLCOM.2021.159560.
[4] R.A. de Groot, F.M. Mueller, P.G.V. Engen, K.H.J. Buschow, New Class of Materials: Half-Metallic Ferromagnets, Phys. Rev. Lett. 50 (25) (1983) 2024–2027.
[5] D.S. Priyanka, J.B. Sudharsan, M. Srinivasan, P. Ramasamy, Cobalt based new quaternary Heusler alloys for Spintronic and thermoelectric applications: an Ab-initio study, Mater. Technol. (2022), https://doi.org/10.1080/10667857.2021.2014030.
[6] S.A. Mir, D.C. Gupta, Understanding the origin of half-metallicity and thermophysical properties of ductile La2CuMnO6 double perovskite, Int. J. Energy Res. 43 (2019) 4783–4796, https://doi.org/10.1002/ER.4620.
[7] S.A. Khandy, D.C. Gupta, Magneto-electronic, mechanical, thermoelectric and thermodynamic properties of ductile perovskite Ba2SmNbO6, Mater. Chem. Phys. 239 (2020), 121983, https://doi.org/10.1016/J.MATCHEMPHYS.2019.121983.
[8] K. Schwarz, CrO2 predicted as a half-metallic ferromagnet, J. Phys. F: Met. Phys. 16 (9) (1986) L211–L215.
[9] H.S. Cherif, A. Bentouaf, Z.A. Bouyakoub, H. Rached, B. Aïssa, Computational determination of structural, electronic, magnetic and thermodynamic properties of Co2HfZ (Z = Al, Ga, Si and Sn) full Heusler compounds for spintronic applications, J. Alloy. Compd. 894 (2022), 162503, https://doi.org/10.1016/J.JALLCOM.2021.162503.
[10] L. Wang, Y. Cao, C. Zhang, Y. Xu, S. Zhou, Theoretical study of structural, mechanical, electronic, magnetic and thermodynamic properties of Cu2MnAl-type Fe2YAl (Y = Cr, Mo and W) full-Heusler alloys, Mater. Sci. Eng., B 278 (2022), 115639, https://doi.org/10.1016/J.MSEB.2022.115639.
[11] G. Surucu, A. Candan, A. Erkisi, A. Gencer, H.H. Güllü, First principles study on the structural, electronic, mechanical and lattice dynamical properties of XRhSb (X = Ti and Zr) paramagnet half-Heusler antimonides, Mater. Res. Express 6 (2019), 106315, https://doi.org/10.1088/2053-1591/AB4039.
[12] G. Surucu, M. Isik, A. Candan, X. Wang, H.H. Gullu, Investigation of structural, electronic, magnetic and lattice dynamical properties for XCoBi (X: Ti, Zr, Hf) Half-Heusler compounds, Phys. B Condens. Matter. 587 (2020), 412146, https://doi.org/10.1016/J.PHYSB.2020.412146.
[13] G. Surucu, A. Gencer, O. Surucu, D. Usanmaz, A. Candan, Pressure and spin effect on the stability, electronic and mechanic properties of three equiatomic quaternary Heusler (FeVHfZ, Z = Al, Si, and Ge) compounds, Mater. Today Commun. 29 (2021), 102941, https://doi.org/10.1016/J.MTCOMM.2021.102941.
[14] M. Shakil, H. Sadia, S.S.A. Gillani, M. Shahid, M. Rizwan, M.A. Gadhi, et al., Computation of Structural, Mechanical, Thermal, and Magnetic Characteristics of Newly Designed Quaternary Heusler Alloys CoNbCrZ (Z = Al, Ga, Si, Ge), J. Supercond. Nov. Magn. 34 (2021) 3243–3254, https://doi.org/10.1007/S10948-021-06066-8/TABLES/6.
[15] Y. Han, M. Wu, M. Kuang, T. Yang, X. Chen, X. Wang, All-d-metal equiatomic quaternary Heusler hypothetical alloys ZnCdTMn (T = Fe, Ru, Os, Rh, Ir, Ni, Pd, Pt): A first-principle investigation of electronic structures, magnetism, and possible martensitic transformations, Results Phys. 11 (2018) 1134–1141, https://doi.org/10.1016/J.RINP.2018.11.024.
[16] J. Ji, Q. Gu, R. Khenata, F. Guo, Y. Wang, T. Yang, X. Tan, Structural configuration and tetragonal phase stability in the equiatomic quaternary Heusler compound TiZnMnSi, RSC Adv. 10 (65) (2020) 39731–39738.
[17] T. Graf, F. Casper, J. Winterlik, B. Balke, G.H. Fecher, C. Felser, Crystal Structure of New Heusler Compounds, Zeitschrift Für Anorg Und Allg Chemie 635 (2009) 976–981, https://doi.org/10.1002/ZAAC.200900036.
[18] S. Yamada, S. Kobayashi, F. Kuroda, K. Kudo, S. Abo, T. Fukushima, T. Oguchi, K. Hamaya, Magnetic and transport properties of equiatomic quaternary Heusler CoFeVSi epitaxial films, Phys. Rev. Mater. 2 (12) (2018), 124403, https://doi.org/10.1103/PHYSREVMATERIALS.2.124403/FIGURES/7/MEDIUM.
[19] G. Wang, C. Li, J. Feng, Z. Zhang, X. Yuan, Y. Liu, S. Song, J. Liu, D. Wang, Z. Lu, R. Xiong, Suppression of Co-Cr antisite defect and robust half metallicity in CoMCrAl (M = Mn, Fe) Heusler alloys, J. Alloy. Compd. 891 (2022) 161856.
[20] D. Rani, J. Kangsabanik, K.G. Suresh, A. Alam, Disorder-mediated quenching of magnetization in NbVTiAl: Theory and experiment, J. Magn. Magn. Mater. 551 (2022), 169124, https://doi.org/10.1016/J.JMMM.2022.169124.
[21] V. Romaka, A. Omar, W. Löser, B. Büchner, S. Wurmehl, Thermodynamic and DFT modeling in quaternary Co-based Heusler phase space: Understanding the interplay between disorder, bonding, and magnetism, Comput. Mater. Sci. 203 (2022), 111089, https://doi.org/10.1016/J.COMMATSCI.2021.111089.
[22] J.-R. Liu, X.-P. Wei, W.-L. Chang, X. Tao, Structural stability, electronic and magnetic properties for half-metallic quaternary Heusler alloys CrLaCoZ, J. Phys. Chem. Solids 163 (2022), 110600, https://doi.org/10.1016/J.JPCS.2022.110600.
[23] M. Shakil, H. Arshad, M. Zafar, M. Rizwan, S.S.A. Gillani, S. Ahmed, First-principles computation of new series of quaternary Heusler alloys CoScCrZ (Z = Al, Ga, Ge, In): a study of structural, magnetic, elastic and thermal response for spintronic devices, Mol. Phys. 118 (2020) 24, https://doi.org/10.1080/00268976.2020.1789770.
[24] Y. Li, G.D. Liu, X.T. Wang, E.K. Liu, X.K. Xi, W.H. Wang, G.H. Wu, L.Y. Wang, X. F. Dai, First-principles study on electronic structure, magnetism and half-

metallicity of the NbCoCrAl and NbRhCrAl compounds, Results Phys. 7 (2017) 2248–2254.
[25] G. Kresse, J. Furthmüller, Efficiency of ab-initio total energy calculations for metals and semiconductors using a plane-wave basis set, Comput. Mater. Sci. 6 (1996) 15–50, https://doi.org/10.1016/0927-0256(96)00008-0.
[26] G. Kresse, J. Furthmüller, Efficient iterative schemes for *ab initio* total-energy calculations using a plane-wave basis set, Phys. Rev. B 54 (16) (1996) 11169–11186.
[27] J.P. Perdew, K. Burke, M. Ernzerhof, Generalized Gradient Approximation Made Simple, Phys. Rev. Lett. 77 (18) (1996) 3865–3868.
[28] G. Kresse, D. Joubert, From ultrasoft pseudopotentials to the projector augmented-wave method, Phys. Rev. B 59 (3) (1999) 1758–1775.
[29] P.E. Blöchl, Projector augmented-wave method, Phys. Rev. B 50 (24) (1994) 17953–17979.
[30] J.D. Pack, H.J. Monkhorst, "Special points for Brillouin-zone integrations"—a reply, Phys. Rev. B 16 (4) (1977) 1748–1749.
[31] Y. Le Page, P. Saxe, Symmetry-general least-squares extraction of elastic data for strained materials from *ab initio* calculations of stress, Phys. Rev. B 65 (2002), 104104, https://doi.org/10.1103/PhysRevB.65.104104.
[32] R. Gaillac, P. Pullumbi, F.-X. Coudert, ELATE: an open-source online application for analysis and visualization of elastic tensors, J. Phys.: Condens. Matter 28 (27) (2016) 275201.
[33] J.W. Jaeken, S. Cottenier, Solving the Christoffel equation: Phase and group velocities, Comput. Phys. Commun. 207 (2016) 445–451, https://doi.org/10.1016/J.CPC.2016.06.014.
[34] A. Togo, I. Tanaka, First principles phonon calculations in materials science, Scr. Mater. 108 (2015) 1–5, https://doi.org/10.1016/J.SCRIPTAMAT.2015.07.021.
[35] A. Gencer, G. Surucu, Properties of BaYO3 perovskite and hydrogen storage properties of BaYO3Hx, Int. J. Hydrogen Energy 45 (2020) 10507–10515, https://doi.org/10.1016/J.IJHYDENE.2019.06.198.
[36] Q. Gao, I. Opahle, H. Zhang, High-throughput screening for spin-gapless semiconductors in quaternary Heusler compounds, Phys. Rev. Mater. 3 (2019), 024410, https://doi.org/10.1103/PHYSREVMATERIALS.3.024410/FIGURES/5/MEDIUM.
[37] E.A. Vasilev, V.A. Virchenko, Solid solutions in the (Fe1.22Sb)1–x(Fe1.68Sn)x system, Phys. Status Solidi 70 (1982) K141–K143, https://doi.org/10.1002/PSSA.2210700259.
[38] J. Ma, V.I. Hegde, K. Munira, Y. Xie, S. Keshavarz, D.T. Mildebrath, et al., Computational investigation of half-Heusler compounds for spintronics applications, Phys. Rev. B 95 (2017), 024411, https://doi.org/10.1103/PHYSREVB.95.024411/FIGURES/19/MEDIUM.
[39] S. Kirklin, J.E. Saal, B. Meredig, A. Thompson, J.W. Doak, M. Aykol, et al., The Open Quantum Materials Database (OQMD): assessing the accuracy of DFT formation energies, npj Comput. Mater. 2015 (11) (2015.1–15) 1, https://doi.org/10.1038/npjcompumats.2015.10.
[40] J.E. Saal, S. Kirklin, M. Aykol, B. Meredig, C. Wolverton, Materials design and discovery with high-throughput density functional theory: The open quantum materials database (OQMD), JOM 65 (2013) 1501–1509, https://doi.org/10.1007/S11837-013-0755-4/FIGURES/7.
[41] K. Özdoğan, E. Şaşioğlu, I. Galanakis, Slater-Pauling behavior in LiMgPdSn-type multifunctional quaternary Heusler materials: Half-metallicity, spin-gapless and magnetic semiconductors, J. Appl. Phys. 113 (2013), 193903, https://doi.org/10.1063/1.4805063.
[42] Y.C. Gao, Y. Zhang, X.T. Wang, Phase stability, band gap, and electronic and magnetic properties of quaternary heusler alloys FeMnScZ (Z = Al, Ga, In), J. Korean Phys. Soc. 2015 (666) (2015.959–65) 66, https://doi.org/10.3938/JKPS.66.959.
[43] M.I. Khan, H. Arshad, M. Rizwan, S.S.A. Gillani, M. Zafar, S. Ahmed, et al., Investigation of structural, electronic, magnetic and mechanical properties of a new series of equiatomic quaternary Heusler alloys CoYCrZ (Z = Si, Ge, Ga, Al): A DFT study, J. Alloy. Compd. 819 (2020), 152964, https://doi.org/10.1016/J.JALLCOM.2019.152964.
[44] F. Mouhat, F.X. Coudert, Necessary and sufficient elastic stability conditions in various crystal systems, Phys. Rev. B 90 (2014), 224104, https://doi.org/10.1103/PhysRevB.90.224104.
[45] M. Born, On the stability of crystal lattices, I. Math Proc Cambridge Philos Soc 36 (1940) 160–172, https://doi.org/10.1017/S0305004100017138.
[46] W. Voigt, Lehrbuch der Kristallphysik, Lehrb Der Krist (1966), https://doi.org/10.1007/978-3-663-15884-4.
[47] A. Reuss, Berechnung der Fließgrenze von Mischkristallen auf Grund der Plastizitätsbedingung für Einkristalle, ZAMM – J. Appl. Math. Mech. / Zeitschrift Für Angew. Math. Und Mech. 9 (1929) 49–58, https://doi.org/10.1002/ZAMM.19290090104.
[48] R. Hill, The Elastic Behaviour of a Crystalline Aggregate, Proc. Phys. Soc. Sect. A 65 (1952) 349, https://doi.org/10.1088/0370-1298/65/5/307.
[49] G. Surucu, A. Candan, A. Gencer, M. Isik, First-principle investigation for the hydrogen storage properties of NaXH3 (X= Mn, Fe, Co) perovskite type hydrides, Int. J. Hydrogen Energy 44 (2019) 30218–30225, https://doi.org/10.1016/J.IJHYDENE.2019.09.201.
[50] A. Gencer, G. Surucu, Investigation of structural, electronic and lattice dynamical properties of XNiH3 (X = Li, Na and K) perovskite type hydrides and their hydrogen storage applications, Int. J. Hydrogen Energy 44 (2019) 15173–15182, https://doi.org/10.1016/J.IJHYDENE.2019.04.097.
[51] D.G. Cahill, S.K. Watson, R.O. Pohl, Lower limit to the thermal conductivity of disordered crystals, Phys. Rev. B 46 (1992) 6131, https://doi.org/10.1103/PhysRevB.46.6131.
[52] D.R. Clarke, C.G. Levi, Materials Design for the Next Generation Thermal Barrier Coatings, Http://DxDoiOrg/101146/AnnurevMatsci33011403113718 2003;33: 383–417. 10.1146/ANNUREV.MATSCI.33.011403.113718.
[53] J. Long, C. Shu, L. Yang, M. Yang, Predicting crystal structures and physical properties of novel superhard p-BN under pressure via first-principles investigation, J. Alloy. Compd. 644 (2015) 638–644, https://doi.org/10.1016/J.JALLCOM.2015.04.229.
[54] M.T. Agne, R. Hanus, G.J. Snyder, Minimum thermal conductivity in the context of diffuson-mediated thermal transport, Energy Environ. Sci. 11 (2018) 609–616, https://doi.org/10.1039/C7EE03256K.